JOURNAL OF GUIDANCE, CONTROL, AND DYNAMICS
Vol. 18, No. 1, January–February 1995

Reduced-Order Model Based Control of the Flexible, Articulated-Truss Space Crane

Brian T. Bansenauer* and Mark J. Balas†
University of Colorado, Boulder, Colorado 80309

The large size and extreme flexibility of an articulated space crane entail tremendous difficulties in precision positioning. We demonstrate the application of a low-order control strategy for the flexible system using a linear, Timoshenko beam finite element model. The model captures the system's low-frequency characteristics. From selected modes of the finite element model, we design a reduced-order model (ROM) controller based on an arbitrary crane configuration. The ROM controller rotates the fixed-shape crane about the base alpha joint to actuate position control. This constructive control design takes place in two pieces: design for performance and compensate for stability. Ignoring the presence of residual modes, we design the low-order control law to achieve our performance criteria. Eigenvalue analysis of the closed-loop system, however, shows the destabilizing interaction of the ROM controller with residuals. Adding a parallel bank of residual mode filters, we restore system stability and performance, without redesign of the original controller. Finally, numeric simulation of the controlled finite element model reveals the effectiveness of a ROM-based control law with residual mode filter compensation. Application to a large-scale data-base highlights the utility of this low-order, noniterative controller design.

Space Crane Control Introduction

THE design of an articulated space crane began under NASA's Pathfinder program. The crane is foreseen as a necessary tool to assemble large structures in space (Fig. 1). It also represents a control problem of great interest, pushing the limits of robotics and flexible structure control. The performance requirements of an articulated crane will be stringent, but the large size and extreme flexibility of the crane create major difficulties in precision positioning. To be useful as a construction tool, the crane must combine quick maneuvering with accurate positioning, as well as safe and stable operation. A rigid-body approximation of the crane is inadequate to meet these control criteria; closed-loop, flexible structure control is essential to achieve the desired performance.

Yet, any control law which tried to capture all of the dynamics involved would be much too complicated to implement in real time. A controller for the articulated space crane must make use of a low-order control strategy. In doing so, however, the interaction of unmodeled structural dynamics with the controller can destabilize the system.[1–3]

As a first step toward control of the articulated crane, we examine the linear, fixed crane system. Here, the crane is given a specific configuration, and the corresponding controller is based on the mode shapes and mode frequencies of the particular crane orientation. The crane maneuvers via rotation about the base, alpha joint (Fig. 2). During operation, this type of slue with all other joints locked could quickly and safely reposition the crane for some new task.

This paper models the three-dimensional truss crane with beam elements. Using beam elements reduces by an order of magnitude the several thousand degrees-of-freedom, full truss model. Although this entails some simplification, control of the beam, finite element model (FEM) concisely and persuasively demonstrates the reduced-order model (ROM)/residual mode filters (RMF) constructive design on a challenging problem. Furthermore, we take care in our reduction to faithfully image, as far as possible, the original truss design given by Sutter and Bush.[4]

Received Feb. 21 1993; revision received Nov. 2, 1993; accepted for publication Jan. 20, 1994.

*Research Assistant, Department of Aerospace Engineering Sciences; currently 1507 Wilson Street, Eau Claire, WI 54701. Member AIAA.

†Professor, Department of Aerospace Engineering Sciences, Box 429. Member AIAA.

Modeling of the Three-Dimensional Truss Crane

Controller design for a linear, flexible crane begins with the development of a FEM. We simplify the three-dimensional truss structure of the space crane to Timoshenko beam elements. The properties for the component pieces of the truss appear in Ref. 4. Combining this with mass distribution data,[5] we construct a finite element beam model, 22 elements in all, with one element for each bay of the space crane. Component properties of the truss are transformed to beam material properties based on an average truss cross-section. We assume linearity of the system under small angle rotations.

Comparing the fundamental frequency of the beam FEM with data for the full three-dimensional truss FEM,[6] one can see that the simplified model captures the low-frequency characteristics of the truss (Table 1) for every configuration. The fundamental frequencies of the two models differ by about 16% for each of the separate comparison configurations.

The Timoshenko beam, lumped model in physical coordinates q, has the following form:

$$M\ddot{q} + D\dot{q} + Kq = Bu, \qquad y = Cq + E\dot{q} \tag{1}$$

The damping in any space structure is rather poorly known, and expected to be quite small. We assume a slight amount of Rayleigh damping, introduced as

$$D = \alpha_1 M + \alpha_2 K \tag{2}$$

Mode shapes ϕ_k and mode frequencies ω_k are calculated from the generalized eigenproblem for Eq. (1):

$$\left(K - \omega_k^2 M\right)\phi_k = 0 \qquad k = 1, \ldots, H \tag{3}$$

where M and K are both symmetric, positive semidefinite (with M positive definite), and have dimension H equal to the number of degrees of freedom (DOF) in the physical model. Modal coordinates z are obtained by the transformation

$$q = \Phi z \tag{4}$$

where $\Phi = [\phi_1, \ldots, \phi_H]$. Typically, the number L of modes computed is much smaller than the number of DOF H included in the physical model; i.e., $L \ll H$. This is done largely to avoid the accumulation of roundoff error in the calculation.

Table 1 Fundamental frequency comparison for different configurations

Configuration	Three-dimentional Truss, Hz	Timoshenko, Hz	Error %
Straight beam	0.135	0.156 Hz	15.7
Joint 3 @ 90 deg	0.136	0.160 Hz	16.0
Joint 2 @ 90 deg	0.103	0.119 Hz	15.5
Joint 1 @ 90 deg	0.085	0.110 Hz	15.5

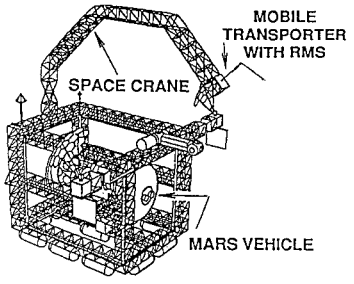

Fig. 1 Space crane operation.

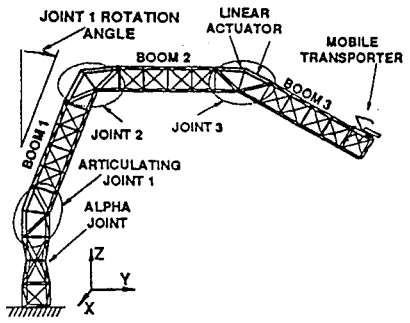

Fig. 2 Space crane truss schematic.

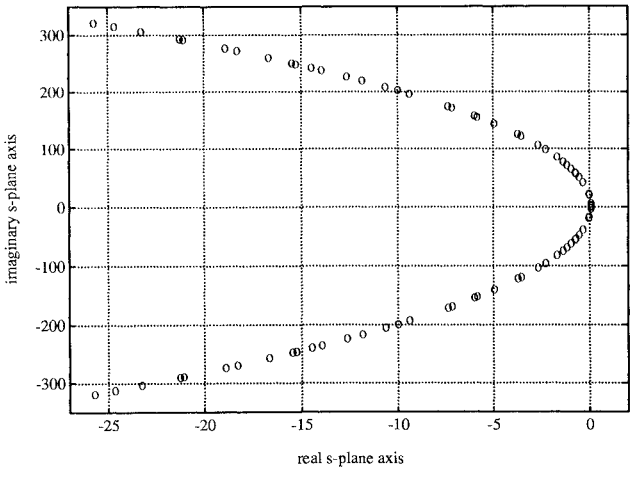

Fig. 3 Space crane open-loop eigenvalues.

To extract a subset of the system's eigenvalues and eigenvectors, we use an orthogonalized factorization technique. The computational procedure developed by R. Quan[7] generates the eigensolution based on the same FEM used for simulation. We compute the 40 lowest eigenvalues and corresponding eigenvectors to form an 80th-order truth model of the crane. Note, although we use only the truth model to establish our controller design, we simulate the control law in closed loop with the full FEM. For a fixed crane configuration, 45-deg rotation at each articulating joint, the system frequencies range from 0.22 Hz to approximately 50 Hz and include the rigid-body motion about the alpha joint (Table 2). Choosing arbitrary Rayleigh damping coefficients (2), $\alpha_1 = 0.0$ and $\alpha_2 = 0.0005$, we generate the open-loop system eigenvalues shown in Figure 3.

Table 2 Truth model frequencies: open loop

No.	Frequency, Hz	No.	Frequncy, Hz	No.	Frequency, Hx%
1	0.0000	16	16.6770	31	39.4281
2	0.2265	17	19.1716	32	39.6715
3	0.6814	18	19.6277	33	41.1958
4	0.7763	19	22.5866	34	43.1608
5	2.9933	20	24.4778	35	43.8706
6	3.3540	21	24.7680	36	46.2857
7	6.4643	22	27.0980	37	46.4850
8	7.8548	23	27.4893	38	48.6184
9	8.8751	24	30.9682	39	50.0688
10	9.0972	25	31.9421	40	51.1199
11	10.2061	26	32.9381		
12	11.2291	27	34.7419		
13	12.0387	28	35.9054		
14	13.3464	29	37.7010		
15	15.4645	30	38.4024		

Fixed-Configuration Controller Design

The analysis and design of the low-order controller is based on the eigenvalue truth model. We handle all of the design and system analysis with the MATLAB™ software package. Let us begin with an overview of our design approach for the fixed crane controller.

First, a ROM is selected from the truth model modes; the modes most important to the performance of the structure are collected into the ROM, as indicated in the following discussion. For this study, we define "performance" as end-effector placement via rotation of the fixed shape crane about the alpha joint. Given our global repositioning objective, we propose that the modes critical to closed-loop performance are the low-frequency ones, most excitable through the base alpha joint. Understand that by using only the base alpha joint actuator, we cannot affect some of the crane's torsional or bending modes: those mode shapes out of plane with respect to actuator motion. However, we directly affect the system's only rigid-body mode, which governs the global angular position of the crane. This suffices to demonstrate the benefits and limitations of our noniterative, low-order controller design.

Consider the continuous-time system in modal coordinates z:

$$\ddot{z} + \alpha_2 \Lambda \dot{z} + \Lambda z = B_0 u, \qquad y = C_0 z + E_0 \dot{z} \tag{5}$$

where $\Lambda \doteq \text{diag}[\omega_1^2, \ldots, \omega_L^2]$ (see Appendix A); B_0 defines how the actuators affect the modes, and C_0 and E_0 describe sensor output in modal terms. In modal coordinates, each open-loop mode is decoupled from all others. Therefore, the selection of the modes most critical to the desired system performance is relatively easy.

The controllability gramian provides a measure for comparing each mode's excitability, i.e., its relative effect on system performance. Looking within the spectrum of low-frequency modes, we collect different modes into a test model and examine the singular values of the model's gramian. Based on each mode's relative effect on performance, we choose the 1st (0.00 Hz), 3rd (0.68 Hz), 5th (3.0 Hz), and 14th (13.3 Hz) mode. These modes form the ROM z_N; all others we consider residual modes z_R. Among the low-frequency modes, those having mode shapes out of plane with respect to actuator motion are excluded from the ROM. Again, the singular values of each mode's controllability gramian provide the measure of actuator sensitivity. We found that, although the 14th mode is separated in frequency from the others, its mode shape is excitable via the base alpha joint.

Let

$$x_N \doteq \begin{bmatrix} z_N \\ \dot{z}_N \end{bmatrix} \quad \text{and} \quad x_R \doteq \begin{bmatrix} z_R \\ \dot{z}_R \end{bmatrix}$$

then the system in state-space form becomes

$$\dot{x}_N = A_N x_N + B_N u \qquad \dot{x}_R = A_R x_R + B_R u$$
$$y = y_N + y_R = C_N x_N + C_R x_R \tag{6}$$

Note that $\dim(z_N) = N$, $\dim(z_R) = R \Rightarrow \dim(z) = N + R = L$; thus $\dim(x_N) = 2N$ and $\dim(x_R) = 2R$. The input/output characteristics of the eighth-order model are compared with the truth model in Fig. 4 .

The design of the ROM-based controller uses a linear quadratic regulator (LQR) augmented with an estimator. The LQR/estimator approach is sensitive to parameter variations from structure to controller design model. No doubt, this will affect the actual system's closed-loop performance. However, the control model uses relatively few, low-frequency modes, which generally have well characterized modal information.

For the LQR design, states are weighted to minimize the position error at the end-effector. Define a cost function as

$$J = \int_0^\infty (y_N' Q y_N + u' R u) dt$$
$$J = \int_0^\infty (x_N' C_N' Q C_N x_N + u' R u) dt \tag{7}$$

where Q and R are symmetric and positive definite. We then define $Q_N = C_N' Q C_N + \varepsilon I$ (with I the identity matrix and $\varepsilon > 0$), to ensure the positive definiteness of Q_N. Our standard quadratic regulator cost function becomes

$$\tilde{J} = \int_0^\infty (x_N' Q_N x_N + u' R u) dt \tag{8}$$

Making use of the deterministic separation principle, we design the control law in two parts: ROM state estimator gains K_N, and ROM state feedback regulator gains G_N. The resulting eighth-order controller follows:

$$u = G_N \hat{x}_N, \qquad \hat{y}_N = C_N \hat{x}_N$$
$$\dot{\hat{x}}_N = A_N \hat{x}_N + B_N u + K_N (y - \hat{y}_N) \tag{9}$$

The LQR design of the controller yields the regulator and estimator gain matrices given in Appendix B, with their design pole positions shown in Fig. 5. The ROM controller would perform perfectly (i.e., with the closed-loop characteristics of the designed poles $A_N + B_N G_N$ and $A_N - K_N C_N$), if the system to be controlled were only the four modes collected into the ROM.

However, because our low-order controller knows nothing about the residual modes z_R, it can interact adversely with some of them. Indeed, from analysis of the truth model in closed loop with the ROM controller,

$$\begin{bmatrix} x_N \\ e_N \\ x_R \end{bmatrix} = \begin{bmatrix} A_N + B_N G_N & B_N G_N & 0 \\ 0 & A_N - K_N C_N & K_N C_R \\ B_R G_N & B_R G_N & A_R \end{bmatrix} \begin{bmatrix} x_N \\ e_N \\ x_R \end{bmatrix} \tag{10}$$

where $e_N \doteq \hat{x}_N - x_N$, we find that residual mode interaction (RMI) degrades system performance, destabilizing the closed loop.

Residual Mode Compensation

Examine the eigenvalues (Fig. 6) of the truth model in closed loop with the ROM controller. Most apparent is an unstable mode at approximately 47 rad/s or 7.5 Hz. Also, note the ROM mode's loss of stability margin from the original design.

With RMFs, we can compensate for RMI, restoring system stability and performance. An iterative method of design might reselect the ROM to include the RMI-sensitive mode. Recall, though, that we based the choice of our ROM on performance specifications. The mode driven unstable has little relevance to how the system performs, except in its effect on closed-loop stability. In fact, the sensitive residual mode is difficult to affect with our actuator, so a control law that included it would require much more gain. Higher gain would introduce greater RMI into the system, conceivably destabilizing another residual mode. Thus, iterating over a larger and larger ROM in no way guarantees arriving at a stable, low-order controller, yet it requires a total redesign at each iteration.

Instead, start with the premise that the ROM-based controller has been effectively designed to establish the necessary performance of the system. Therefore, no redesign of the ROM control law is needed. To remove the de-stabilizing RMI, add second-order residual mode filters around the ROM controller (see Fig. 7). The addition of RMF compensation is straightforward, noniterative, and experimentally tested.[8] Its only difficulty involves ascertaining all of

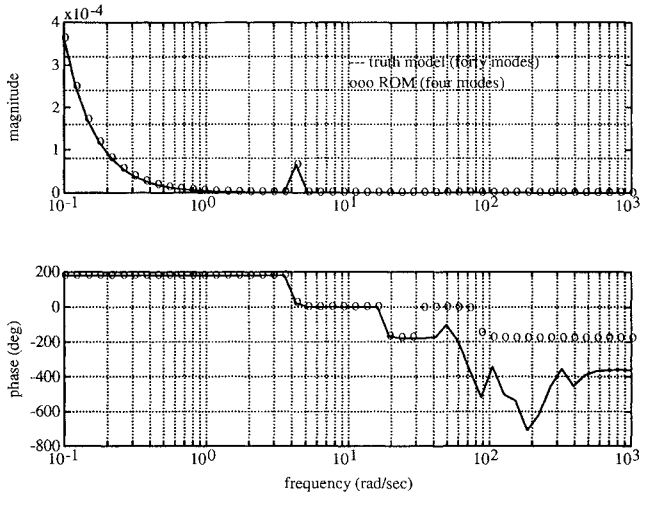

Fig. 4 Frequency response: actuator to tip sensor % (x-position).

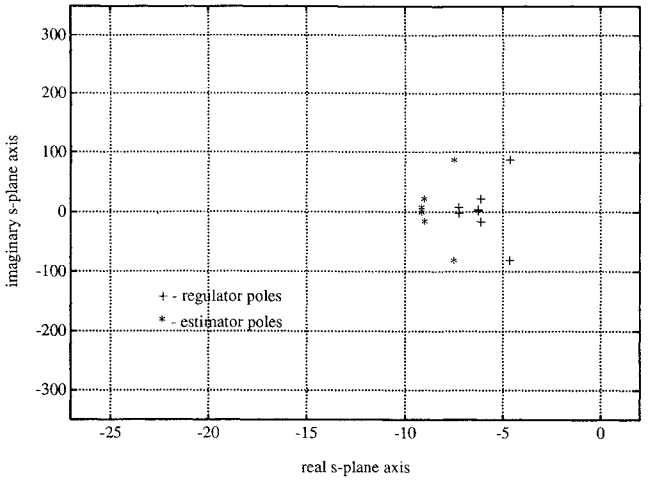

Fig. 5 ROM controller design pole positions.

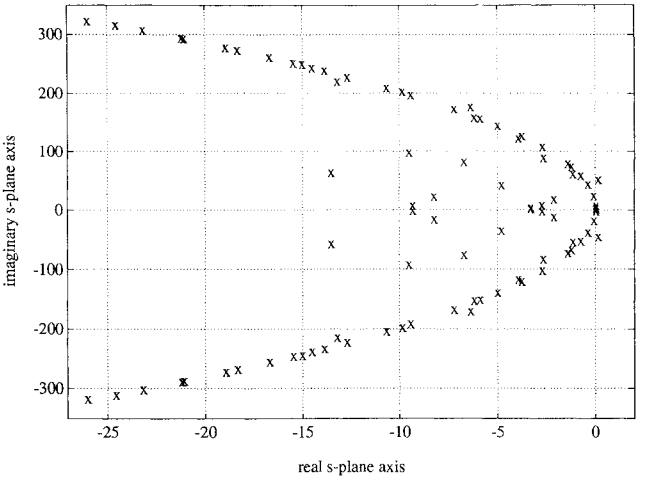

Fig. 6 ROM control, closed-loop eigenvalues.

Table 3 Residual modes for RMF compensation

Mode	Pole location	Frequency, Hz
8	$-0.609 \pm j\ 49.3$	7.855
15	$-2.360 \pm j\ 97.1$	15.465
17	$-3.628 \pm j\ 120.4$	19.172
27	$-11.913 \pm j\ 218.0$	34.742
29	$-14.028 \pm j\ 236.5$	37.701

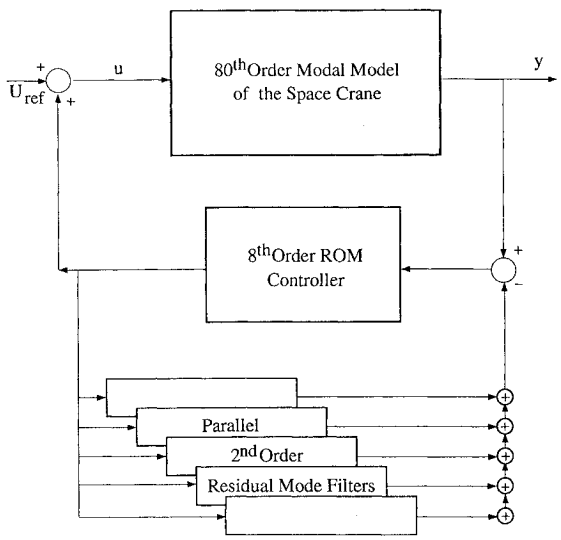

Fig. 7 Space crane linear controller schematic.

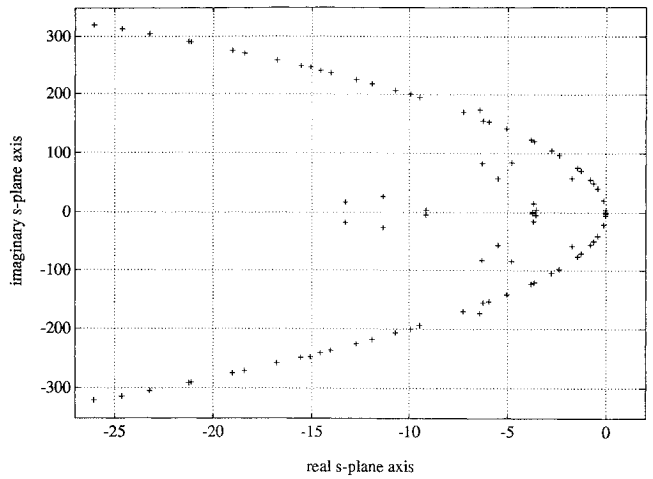

Fig. 8 ROM/RMF control, closed-loop eigenvalues.

the modes defined[1] as Q-modes; analytical and experimental methods to identify these modes have gained ground on this point.[9,10] Once uncovered, the compensation of all Q-modes guarantees the closed-loop stability of the composite controller/compensator[1]; see Appendix C for an abbreviated proof.

RMF design, then, primarily consists of choosing the residual modes to compensate; we construct the RMFs to model residual modes extremely susceptible to interaction with the ROM controller. By examining the terms in Eq. (10) that couple the control law to the residual modes, $B_R G_N$ and $K_N C_R$, we select the most affected residual modes. To ensure we have included all Q-modes, we analyze the closed-loop system without these sensitive modes; its eigenvalues have been shown[2] to determine the stability of the combined ROM/RMF controller. The procedure is constructive, not iterative: remove another highly affected mode, and test the remaining modes in closed loop for stability. No redesign of the original ROM controller occurs.

Initially we select five modes from among the residuals (Table 3). The eigenvalues of the ROM with RMI compensation (Fig. 8), show

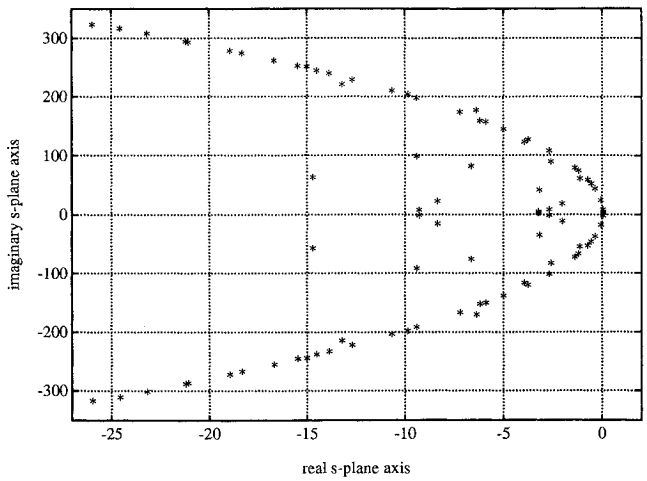

Fig. 9 ROM/RMF control—one residual mode filter.

that the RMFs stabilize the closed loop and restore stability margin to the ROM modes. Although five residual mode filters produce an acceptable design, we experiment with different subsets of these modes. Compensating only the 7.9-Hz mode actually stabilizes the system (Fig. 9), but the stability margin of the ROM modes decreases slightly.

Finally, the ROM controller with RMF compensation remains as implementable in real-time as the ROM controller alone. The addition of several RMFs leaves the ROM controller unchanged; residual mode filters operate in an inherently parallel fashion, and are simple, second-order filters. However, because they contain mode shape, as well as frequency information, they do not merely notch a frequency. By reproducing and canceling the contribution to sensor output from troublesome residual modes, RMFs restore the degraded performance characteristics of the ROM controller, while stabilizing the system. Conceptually, RMF compensation makes the structure seem more like the design model to the ROM controller. The low-order controller views the structure through a pair of rose-colored glasses. Thus, we present the constructive design, and the analysis of an eighth-order ROM with RMF compensation to control an 80th-order plant.

Simulation Results

We employ two computational packages for the simulation of our fixed-crane system. The linear simulation[7] allows the addition of a linear, continuous time control law to close the loop around a FEM. It uses an unconditionally stable integration algorithm; unbounded output represents strictly controller-induced instability. The nonlinear package,[11] however, can only simulate the FEM's open-loop response. We first compare an independent FEM for each simulation routine, using open-loop responses to a small initial velocity. The crane is configured in the y-z plane, with an out-of-plane velocity prescribed at the tip. Time traces for two configurations, a straight arm and our controller design configuration, appear in Figs. 10 and 11. Here, the locked configuration crane operates well within its linear range. The traces show the compatibility of the two FEMs under identical initial conditions.

Simulation of the linear controller, in closed loop with the FEM provides further insight into the ROM/RMF design. Here we compare traces for the ROM-based control law, with and without compensation. Recall analysis of the truth model with ROM control reveals an unstable mode at 7.5 Hz. Simulation of the FEM with ROM control bears the analysis out; the angular velocity about the Z axis (Fig. 12a) illustrates the destabilizing effect of RMI. Compensating for five residual modes (Fig. 12b) restores system stability.

Notice however (see Table 3), we never filter the 7.5-Hz signal; RMF design uses only modal information extracted from the original model, or, in some cases, obtained experimentally. Whether or not we add RMFs, the simulation shows a 7.5-Hz mode excited

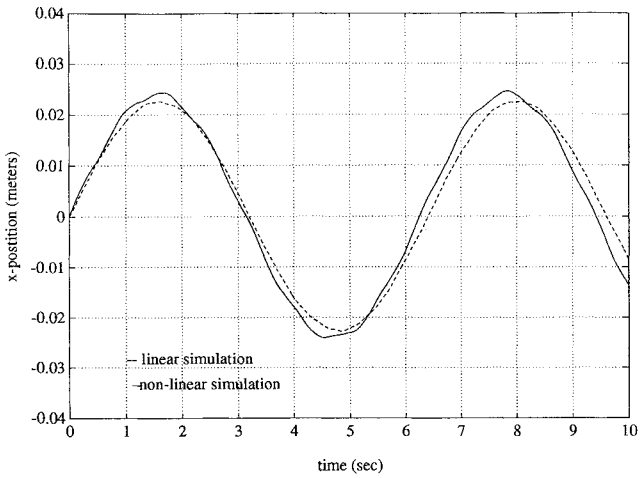

Fig. 10 Tip response to a small initial velocity.

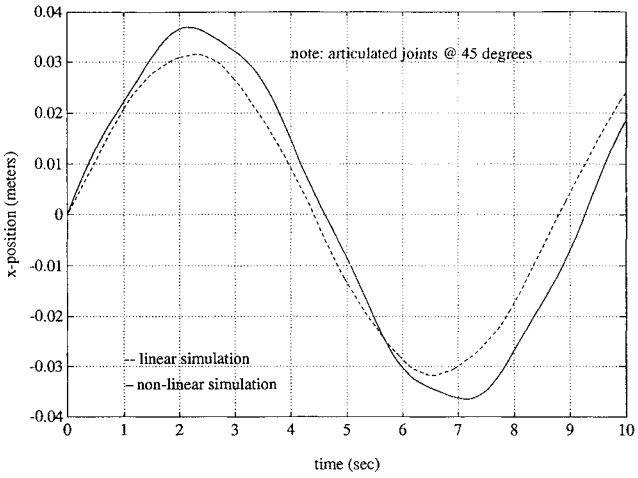

Fig. 11 Tip response to a small initial velocity.

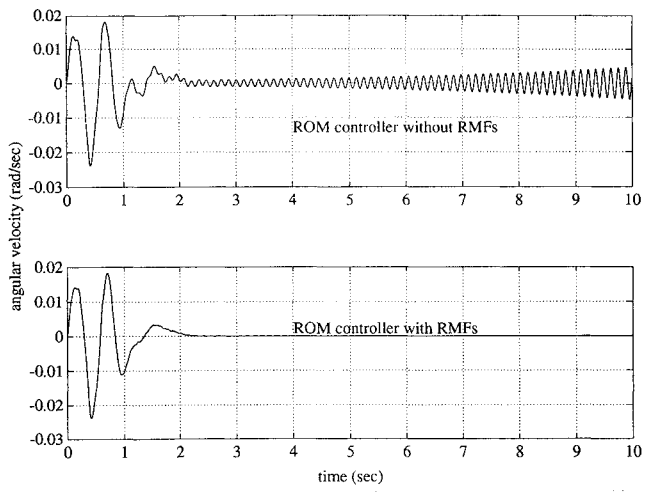

Fig. 12 Closed-loop tip velocity (x direction) with and without RMI compensation.

by the ROM controller during its first second of operation (see Fig. 12). However, with RMF compensation the excitation decays as it would in the open-loop system; without it, the residual mode interacts with the ROM controller and the oscillation grows. The performance of the ROM/RMF controller stands out in comparison to the open-loop system given the same step command (Fig. 13).

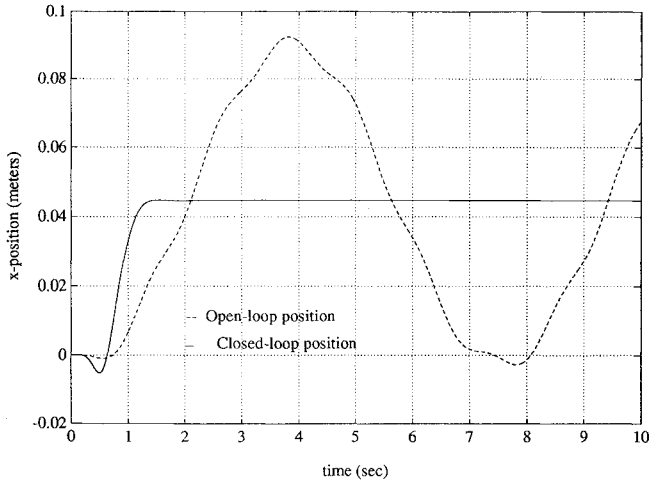

Fig. 13 Tip response to a small angle slue command.

Conclusions

Most of the work to date for control of the space crane[5,12] assumes that it either moves very slowly or that it is very stiff. Both of these rigid-body assumptions are good starting points; however, it seems clear that the flexible nature of the crane must now be considered. We begin the design of a control algorithm for the fixed configuration crane by developing a beam model to capture the low-frequency behavior of the full three-dimensional truss.

Next, we step through the design of both the ROM controller and RMF compensation. We discuss the details of selecting ROM modes, as well as those residuals needing compensation. The progressive method of design, which constructs a ROM control law for performance then compensates for stability, proves simple and effective. This general ROM design, distinguishing performance from stability, sets it apart from other ROM based approaches.

We examine the FEM using results from a linear and nonlinear simulation procedure for the open-loop system. Traces from the linear, closed-loop simulation give deeper insight to the nature of RMF compensation, i.e., RMFs do not notch out undesirable frequencies but extend the reduced-order control model without iterating. Lastly, this work demonstrates again the applicability of ROM/RMF control on a sizable model of a most interesting, large-space structure.

Acknowledgments

Our appreciation to the Center for Space Structures and Controls, NASA Grant NAG-1-756, for computer hardware and software support. We would like to thank Janice Downer for her time and effort in explaining and modifying her nonlinear beam code. Please note that Figs. 1 and 2 are taken from Sutter et al.

Appendix A: Truth Model

Table A1 Λ diagonal entries

No.	Entry	No.	Entry	No.	Entry
1	0.0000e−00	16	1.4510e+04	31	5.6113e+04
2	2.0251e+00	17	1.0980e+04	32	6.1372e+04
3	1.8328e+01	18	1.5209e+04	33	7.5981e+04
4	3.5372e+02	19	2.4218e+04	34	7.3542e+04
5	2.3790e+01	20	2.0140e+04	35	6.6999e+04
6	4.4412e+02	21	2.9832e+04	36	6.2132e+04
7	2.4357e+03	22	2.3654e+04	37	3.7861e+04
8	1.6497e+03	23	2.8989e+04	38	5.8221e+04
9	3.2672e+03	24	4.0280e+04	39	5.0895e+04
10	4.1123e+03	25	1.0317e+05	40	4.2831e+04
11	3.1096e+03	26	9.8968e+04		
12	7.0322e+03	27	9.3317e+04		
13	9.4414e+03	28	4.7651e+04		
14	4.9779e+03	29	8.5307e+04		
15	5.7216e+03	30	8.4577e+04		

Table A2 B_0 entries for alpha joint actuator

No.	Entry	No.	Entry	No.	Entry
1	2.2371e−04	16	1.7071e−03	31	−8.8483e−03
2	−8.2403e−19	17	9.7550e−18	32	1.9922e−03
3	6.3717e−04	18	−1.4886e−18	33	−8.5603e−10
4	7.3159e−04	19	−1.1042e−03	34	2.7769e−09
5	1.2033e−19	20	5.8207e−18	35	6.0789e−11
6	−2.5433e−18	21	−6.6065e−03	36	−2.0519e−11
7	6.3678e−04	22	−9.3994e−18	37	−7.6560e−18
8	−9.9662e−19	23	−1.8059e−17	38	−1.9545e−12
9	1.3723e−04	24	−8.4282e−03	39	2.8567e−15
10	1.3164e−03	25	−3.3611e−03	40	−2.4495e−17
11	−1.8007e−17	26	2.9058e−03		
12	−3.9323e−03	27	1.2774e−03		
13	5.8510e−03	28	−4.1903e−03		
14	6.5255e−18	29	−3.0820e−03		
15	−2.9752e−18	30	−2.5333e−03		

Table A3 C_0 entries for position sensors

Hub angular positiion	Joint 1 X-position	Joint 3 X-position	Tip Y-position	Tip Z-position	Tip X-position
2.2371e−04	−1.6787e−09	1.1457e−02	−2.3471e−18	−1.2533e−17	1.6203e−02
−8.2397e−19	−3.4016e−18	−1.8341e−17	−3.0856e−03	−1.6476e−02	−6.7803e−18
6.3717e−04	7.0161e−04	2.0354e−02	4.6302e−18	−1.1943e−17	−1.0264e−02
7.3159e−04	4.2269e−03	−2.2118e−02	−9.0974e−19	−7.3244e−18	5.9763e−03
1.2802e−19	−1.1177e−17	2.1761e−17	−1.5905e−02	−1.5664e−03	−7.3812e−18
−2.5202e−18	3.9269e−18	−2.9421e−17	6.9560e−03	4.1462e−03	−4.4711e−18
6.3679e−04	−2.1783e−02	−4.3021e−03	1.3787e−17	−3.3025e−18	4.6941e−03
4.1768e−19	7.0760e−17	3.5164e−17	5.5381e−03	−7.7770e−04	4.3811e−18
1.3723e−04	1.0452e−03	−8.1983e−03	−3.4252e−17	−7.4159e−17	−7.8892e−03
1.3164e−03	−1.7258e−02	−9.3271e−03	−7.7544e−18	−1.8353e−17	−9.9623e−03
−2.5343e−17	1.8374e−17	−8.3374e−17	4.9136e−03	1.0027e−02	−7.5366e−17
−3.9324e−03	2.2232e−02	−1.4835e−02	−1.1477e−17	−6.7826e−18	−6.6262e−03
5.8512e−03	−2.0293e−02	−7.7875e−03	1.7510e−17	6.8689e−18	−3.9353e−03
1.5290e−17	−1.5806e−17	6.4487e−18	7.2531e−03	2.7414e−03	−1.6447e−18
−2.1633e−17	3.5400e−18	−3.4266e−18	−1.1922e−04	7.3491e−03	−1.2574e−18
1.7072e−03	−2.8864e−03	−2.2089e−02	−1.4922e−18	3.4659e−19	5.2219e−03
−1.4963e−17	−2.4887e−17	3.6844e−19	−8.1963e−03	−1.5117e−03	−3.3926e−18
1.8314e−17	9.2277e−18	2.9063e−18	2.1255e−03	−4.9732e−03	3.8081e−18
−1.1043e−03	4.8451e−03	8.1290e−03	−8.4457e−18	2.8893e−18	−4.7527e−04
5.3938e−18	3.23763−18	2.5039e−17	3.8990e−04	−2.9047e−03	5.2455e−19
−6.6071e−03	1.5402e−02	−1.3183e−02	5.7347e−18	1.3398e−18	9.7441e−04
3.4549e−17	3.3687e−17	−1.5438e−17	−4.2213e−03	4.3579e−03	1.6451e−18
1.6484e−18	−1.2936e−17	−3.2778e−17	−6.7999e−04	−1.9441e−03	2.6338e−18
−8.4293e−03	2.3999e−02	−1.9789e−03	9.1813e−18	−1.0967e−17	−8.7726e−04
−3.3622e−03	−7.5553e−05	1.2091e−02	−2.5602e−07	3.1843e−07	−1.8375e−04
2.9067e−03	−1.0431e−02	7.9278e−03	−5.7563e−08	7.1682e−08	−1.3147e−04
1.2778e−03	8.8755e−03	1.3337e−02	−1.9661e−08	2.4544e−08	−4.1949e−04
−4.1909e−03	1.2864e−02	2.1363e−02	5.8464e−18	3.9275e−20	1.1246e−03
−3.0828e−03	−1.3609e−02	−3.2731e−03	9.0207e−11	−1.1342e−10	3.9840e−04
−2.5340e−03	−1.4207e−02	1.2431e−03	−3.3547e−10	4.2268e−10	−6.0365e−04
−8.8498e−03	1.3740e−03	−1.0321e−03	7.9702e−18	−1.1319e−17	−3.0616e−05
1.9925e−03	−1.1706e−02	1.4780e−02	1.3109e−15	−1.5733e−15	3.5959e−04
−8.5631e−10	−6.2354e−10	5.3861e−09	−1.4706e−03	1.0768e−03	−9.1947e−11
2.7778e−09	2.0075e−09	−1.7249e−08	1.0133e−02	−9.9376e−03	2.9303e−10
6.0808e−11	4.3242e−11	−3.6871e−10	4.7661e−03	−5.2892e−03	6.2123e−12
−2.0525e−11	−1.4461e−11	1.2300e−10	−2.1707e−03	−3.0154e−03	−2.0645e−12
−2.0224e−16	1.6442e−17	4.8954e−18	−3.4110e−03	4.0723e−03	−1.4678e−18
−1.9553e−12	−1.3690e−12	1.1631e−11	−3.0385e−03	−1.4280e−03	−1.9478e−13
2.6399e−15	1.9745e−15	−1.6833e−14	2.5461e−03	−3.6196e−03	2.7937e−16
−8.3835e−17	6.6667e−18	6.6800e−17	−3.9967e−03	1.5765e−03	−9.7232e−19

Note: $E_0 = 0$.

Appendix B: Controller Gains

Table B1 Regulator and estimator gains

Regulator Gains	Esimator Gains ($\times 10^4$)					
−8.8256e + 05	0.0016	0.0037	0.0513	0.0000	0.0000	0.0812
−2.5844e + 05	0.0064	0.0180	0.0978	0.0000	0.0000	−0.0558
−4.1154e + 05	0.0050	0.0207	−0.0395	0.0000	0.0000	0.0099
6.2637e + 04	−0.0059	0.0336	−0.0202	0.0000	0.0000	−0.0102
−4.6308e + 05	0.0068	0.0178	0.2095	0.0000	0.0000	0.3820
9.8748e + 04	0.0304	0.0941	0.3082	0.0000	0.0000	−0.2022
5.7167e + 02	−0.0531	−0.1472	−1.5721	0.0000	0.0000	0.4445
1.3198e + 03	−0.0028	0.0842	−0.7657	0.0000	0.0000	−0.1077

Appendix C: Abbreviated Stability Proof for ROM/RMF Controller

The proof here continues from our examination of the closed-loop system in under "Fixed-Configuration Controller Design." Define A_C as the system matrix of Eq. (10); this describes the ROM controller (9) in closed-loop with the plant (6). If A_C is of reasonable size, we compute its eigenvalues to determine closed-loop stability. Otherwise, we can use perturbation techniques.

Because the controller is based on a ROM, it interacts with unmodeled structure dynamics, represented here as the residual modes of (6). Controller/structure interaction occurs through the terms $B_R G_N$ and $K_N C_R$; RMI can cause deterioration of the design performance, reduced stability margin and even instability. Should the analysis of the matrix A_C show the closed-loop system to be stable, with an acceptable stability margin in the z_N modes, then the design is finished. Often however, we must provide compensation for RMI.

RMI occurs as a result of the controller's limited knowledge of the plant, and thus is inevitable whenever we discard residual modes from the control model. However, some residual modes interact more severely with the ROM controller than others. Consider an alternative partitioning of the open-loop, modal system (5), which discriminates these modes. We keep the same ROM modes (z_N); the original ROM controller gains ($G_N K_N$) are left unchanged. But we select some modes (z_Q) and group them separately from the rest of the residual modes (z_R). The state-space representation of the open-loop system follows:

$$\dot{x}_N = A_N x_N + B_N u \tag{C1a}$$

$$\dot{x}_Q = A_Q x_Q + B_Q u \tag{C1b}$$

$$\dot{x}_R = A_R x_R + B_R u \tag{C1c}$$

$$\begin{aligned} y &= y_N + y_Q + y_R \\ &= C_N x_N + C_Q x_Q + C_R x_R \end{aligned} \tag{C1d}$$

Observe that the system dimensions become $\dim(x_N) = 2N$, $\dim(x_Q) = 2Q$, $\dim(x_R) = 2R$ where $N + Q + R = L$.

The Q-modes are often the structural modes most affected by RMI, and thus can be easily extracted from among the other residual modes based on their behavior under closed-loop, control stability analysis. To understand the definition of these troublesome modes, consider that we want the closed-loop system consisting of the structure without the x_Q modes (C1a) and (C1c), together with the original ROM controller (9), to be stable. Therefore, we define as Q-modes all the modes we must remove from the closed-loop system to stabilize it.

In other words, since A_C is not stable, begin to remove the residual modes affected most by RMI until the pared-down system becomes stable. Redefine all "deleted" residual modes as x_Q, and all that remain in the new, stable closed-loop matrix as x_R. Note that we have changed the definition of A_R, B_R, and C_R; they represent the original residuals given in (10) but with the Q-modes extracted. Once the Q-modes are resolved, the RMF design is easily completed. The RMF takes shape as a parallel bank of second-order filters, with A_Q stable:

$$\begin{cases} \dot{\hat{x}}_Q = A_Q \hat{x}_Q + B_Q u \\ \hat{y}_Q = C_Q \hat{x}_Q \end{cases} \tag{C2}$$

Now we examine the structure in closed-loop with the ROM controller (9) and the RMF compensator (C2), as shown in Fig. 7. First, append the ROM with the RMF to obtain the new controller:

$$\begin{cases} u = G_N \hat{x}_N \\ \dot{\hat{x}}_N = A_N \hat{x}_N + B_N u + K_N (y - \hat{y}) \\ \dot{\hat{x}}_Q = A_Q \hat{x}_Q + B_Q u \\ \hat{y} = \hat{y}_N + \hat{y}_Q = C_N \hat{x}_N + C_Q \hat{x}_Q \end{cases} \tag{C3}$$

The innovations term that updates the estimator is now $(y - \hat{y}_N - \hat{y}_Q)$ instead of $(y - \hat{y}_N)$; thus, input to the ROM controller is screened from the effect of Q-modes.

Compiling the closed-loop system matrix A_C^* for the structure (C1) under ROM/RMF control (C3), we have

$$\begin{bmatrix} \dot{x}_N \\ \dot{e}_N \\ \dot{x}_R \\ \dot{x}_Q \\ \dot{e}_Q \end{bmatrix} = \begin{bmatrix} A_N + B_N G_N & B_N G_N & 0 & 0 & 0 \\ 0 & A_N - K_N C_N & K_N C_R & 0 & -K_N C_Q \\ B_R G_N & B_R G_N & A_R & 0 & 0 \\ B_Q G_N & B_Q G_N & 0 & A_Q & 0 \\ 0 & 0 & 0 & 0 & A_Q \end{bmatrix} \times \begin{bmatrix} x_N \\ e_N \\ x_R \\ x_Q \\ e_Q \end{bmatrix} \tag{C4}$$

where $e_N \doteq \hat{x}_N - x_N$ and $e_Q \doteq \hat{x}_Q - x_Q$. Next, consider the following definitions:

$$A_{11}^* \doteq \begin{bmatrix} A_N + B_N G_N & B_N G_N & 0 \\ 0 & A_N - K_N C_N & K_N C_R \\ B_R G_N & B_R G_N & A_R \end{bmatrix}$$

$$A_{13}^* \doteq \begin{bmatrix} 0 \\ -K_N C_Q \\ 0 \end{bmatrix}$$

$$A_{21}^* \doteq [B_Q G_N \quad B_Q G_N \quad 0]$$

$$x_c \doteq [x_N \quad e_N \quad x_R \quad x_Q \quad e_Q]' \tag{C5}$$

Now the overall structure of the closed-loop system

$$\dot{x}_c = \begin{bmatrix} A_{11}^* & 0 & A_{13}^* \\ A_{21}^* & A_Q & 0 \\ 0 & 0 & A_Q \end{bmatrix} x_c \tag{C6}$$

reveals a block zero form. As a result, $\det(sI - A_C^*) = \det(sI - A_{11}^*)\det(sI - A_Q)\det(sI - A_Q)$. Thus, closed-loop stability depends entirely upon the stability of A_{11}^* and A_Q.

First of all, the upper left block, A_{11}^*, of the system matrix represents the structure with x_Q modes deleted, (C1a) and (C1c), in closed-loop with the ROM controller (9). But from the definition of Q-modes, we know that the closed-loop system associated with A_{11}^* is stable. Secondly, all residual modes must necessarily have some inherent, open-loop damping. Remember, they were not collected into the ROM, and therefore were not defined as critical to system performance. Because the Q-modes are selected from among residual modes, the open-loop system (C1b) must be stable, and thus A_Q must be stable. This completes the abbreviated proof of ROM/RMF stability.

One final point concerns the performance of this ROM/RMF controller (C3). Recall that the initial partitioning of the plant (6) gathers together all modes (z_N) critical to our performance objective. The ROM-based control works to shape the output of these modes, but its interaction with residual modes impairs its effectiveness. By compensating for RMI, the ROM/RMF controller not only guarantees closed-loop stability, but also improves the integrity of the designed performance.

References

[1]Balas, M., "Finite-Dimensional Controllers for Linear Distributed Parameter Systems: Exponential Stability Using Residual Mode Filters," Journal of Mathematical Analysis and Application, Vol. 133, 1988, pp. 283–296.

[2]Balas, M., Quan, R., Davidson, R., and Das, B., "Low-Order Control of Large Aerospace Structures Using Residual Mode Filters," *Proceedings of American Controls Conference*, 1988.

[3]Reisenauer, B., Balas, M., and Ramey, M., "Reduced-Order Model Based Control of Large Flexible Manipulators: Theory and Experiments," *Proceedings of the American Controls Conference*, May 1990.

[4]Sutter, H., and Bush, H., "A Comparison of Two Trusses for the Space Station Structure," NASA TM-4093, March 1989.

[5]Gawronski, W., and Ih, C.-H. C., "3D Rigid Body Dynamic Modeling of Space Crane for Control Design and Analysis," NASA JPL D-6878, Nov. 1989.

[6]Sutter, H., Bush, H., and Wallsom, R., "An Articulated-Truss Space Crane Concept," AIAA Paper 90-0994, April 1990.

[7]Quan, R., "Numerical Simulation of Large, Actively Controlled Space Structures," Ph.D. Dissertation, Univ. of Colorado, Boulder, CO, 1990.

[8]Reisenauer, B., "C.S.I. Compensation for Reduced-Order Model Based Control of a Flexible, Robot Manipulator," M.S. Thesis, Univ. of Colorado, Boulder, CO, 1990.

[9]Davidson, R., Balas, M., and Reisenauer, B., "Adaptive CSI Compensation for Reduced-Order-Model-Based Control of a Flexible Robot Manipulator," *Proceedings of the American Controls Conference*, May 1990.

[10]Gooyabadi, A., "Hybrid Actuation," Ph.D. Dissertation, Univ. of Colorado, Boulder, CO, Aug. 1992.

[11]Downer, J., "A Computational Procedure for the Dynamics of Flexible Beams within Multibody Systems," Ph.D. Dissertation, Univ. of Colorado, Boulder, CO, 1990.

[12]Park, K., Chiou, J.C., Downer, J., Farhat, C., Chen, G., and Wada, B. "Dynamics of Three-Dimensional Space Crane: Motion Requirements and Computational Considerations," Amercian Society of Mechanical Engineers Winter Annual Meeting, Paper 90-WA/Aero-7, Nov. 1990.